Available at www.sciencedirect.com

ScienceDirect

journal homepage: www.elsevier.com/locate/he

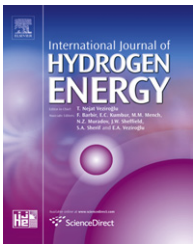

# Pt–Sn/γ-$Al_2O_3$ and Pt–Sn–Na/γ-$Al_2O_3$ catalysts for hydrogen production by dehydrogenation of Jet A-1 fuel: Characterisation and preliminary activity tests

*Carlo Resini* [a,*], *Carlo Lucarelli* [b], *Melanie Taillades-Jacquin* [a], *Kan-Ern Liew* [a,c], *Ilenia Gabellini* [d], *Stefania Albonetti* [b], *David Wails* [d], *Jacques Rozière* [a], *Angelo Vaccari* [b], *Deborah Jones* [a]

[a] *Institut Charles Gerhardt UMR 5253, Agrégats, Interfaces et Matériaux pour l'Energie, Université Montpellier 2, Place Eugène Bataillon, 34095 Montpellier Cedex 5, France*

[b] *Dipartimento di Chimica Industriale e dei Materiali, Alma Mater Studiorum, Università degli Studi di Bologna, Viale del Risorgimento 4, 40136 Bologna, Italy*

[c] *Power Generation, EADS Innovation Works, Dept. IW-EP, Energy & Propulsion, 81663 Munich, Germany*

[d] *Johnson Matthey Technology Centre, Blount's Court, Sonning Common, Reading RG4 9NH, United Kingdom*

ARTICLE INFO

*Article history:*
Received 8 December 2010
Received in revised form
4 February 2011
Accepted 6 February 2011
Available online 21 March 2011

*Keywords:*
Hydrogen
Partial dehydrogenation
Pt–Sn catalysts
Fuel cell
Jet-A-1 fuel

ABSTRACT

The partial dehydrogenation of fuels like diesel or kerosene cuts to produce $H_2$ is an emerging idea of increasing interest. In the present work the study of the partial dehydrogenation of Jet A-1 fuel on Pt–Sn/γ-$Al_2O_3$ based catalysts to produce $H_2$ to feed an on-board (aircraft) proton exchange membrane fuel cell is presented. Extensive physico-chemical characterization of 5% wt.Pt-1% wt.Sn/γ-$Al_2O_3$ and 5%wt.Pt-1%wt.Sn-1%wt.Na/γ-$Al_2O_3$ pelleted materials has been performed. A gradient of the active metals from the edge to the centre of the pellet has been observed. A higher concentration of $Pt^0$ has been detected on the outer part of the pellet than in the inner part, whereas Sn has been detected only on the external part of the pellet. The investigated materials are active as catalysts for the partial dehydrogenation of normal and desulfurised Jet A-1 kerosene fuel. The presence of sulfur compounds and coke deposition strongly affects the $H_2$ productivity which decreases rapidly with time on stream. The presence of a Na cation addition contributes to give the highest and most sustained $H_2$ production. The condensed outlet liquid stream retains the fuel properties in the range of the Jet A-1 kerosene fuel. These are encouraging preliminary results, inviting further research; coking and sulfur poisoning as well as identification of appropriate reaction conditions are the main challenges to be overcome in the immediate future.



## 1. Introduction

The use of fuel cells in transport applications either for propulsion or as an auxiliary power unit will contribute to emissions reductions. In addition to the durability and cost issues, incumbent on fuel cells, efficient on-board $H_2$ storage and production technologies require further development [1–6]. Various methods of $H_2$ storage are being considered,

* *Corresponding author*. Tel.: +33 467143256.
E-mail address: Carlo.Resini@univ-montp2.fr (C. Resini).

0360-3199/$ – see front matter 
doi:10.1016/j.ijhydene.2011.02.036

amongst which liquid and highly-pressurised hydrogen are already at engineering prototype stage whereas solid-state storage as hydrides and porous solid adsorption of molecular $H_2$ are still at early stage of development [3,7,8]. A promising method for storing and transporting $H_2$ is the dehydrogenation of cyclic hydrocarbons with high $H_2$ content, known also as "chemical hydrides" or "organic hydrides" that can be dehydrogenated and hydrogenated reversibly [6,9–12]. In particular, cyclohexane and decalin are considered suitable $H_2$ storage media, their $H_2$ content (7.3% wt., 64.8 kg $H_2/m^3$ for decalin and 7.2 % wt., ~55 kg $H_2/m^3$ for cyclohexane) [6] meeting the US Department of Energy hydrogen storage target for transportation for 2010 (6.0 wt%, 45.0 kg $H_2/m^3$) [4]; but not that for 2015 (9.0 wt%, 81.0 kg $H_2/m^3$) [1].

The use of fuels like diesel or kerosene cuts as $H_2$ source is an emerging idea of increasing interest [13,14]. The aim is to further upgrade an already valuable energy carrier, fossil fuel, by extracting another energy carrier, $H_2$. The lack of oxygen in diesel and kerosene molecular composition makes them suitable for partial dehydrogenation to produce dehydrogenated hydrocarbons in the liquid phase and hydrogen in the gas phase. Since the gas stream is free of carbon oxides, it can be directly fed without any further purification to an on-board proton exchange membrane fuel cell to supply electrical energy to auxiliary systems in maritime and aeronautic applications. It is note worthy that the liquid mixture comprising partially dehydrogenated hydrocarbons still maintains its original fuel properties, so making hydrocarbon mixtures an appealing $H_2$ storage medium. In principle the same catalysts currently employed for dehydrogenation or reforming of hydrocarbons, which are alumina-supported Pt-based mono- or bimetallic catalysts [15] are also suitable for $H_2$ production by hydrocarbon partial dehydrogenation.

Studies have been performed on several different supported metal catalysts for cycloalkane dehydrogenation [6]. Ni and Pt are among the most used active phases [10,14,16–23]. Ni is much cheaper than Pt but its selectivity to dehydrogenation reactions is lower and cracking reactions are more favoured at high temperature. Also the support plays a key role, and the influence of supports such as alumina [10,14,17,21], alumina-sulfated zirconia [14], silica [24], activated carbon [12,19,20,22], carbon nanofibers [9,25,26] or carbon nanotubes [23] has been investigated.

The choice of the catalyst for hydrocarbon dehydrogenation capable of producing $H_2$ without compromising the original fuel properties is crucial. The right catalyst has to favour dehydrogenation or reforming (isomerisation, cyclisation, aromatisation) reactions, while avoiding polymerisation or cracking reactions responsible for coke deposition and catalyst deactivation.

Bimetallic Pt–Sn/$\gamma$-$Al_2O_3$ based catalysts have been widely studied. According to the literature, the presence of Sn inhibits sintering of Pt clusters, improves catalyst stability towards deactivation by coking, and restrains hydrocracking, hydrogenolysis, hydrogenation, and isomerisation, while improving dehydroisomerisation and dehydrocyclisation reactions [14,27–30]. Furthermore, studies on the effect of the addition of alkali metals as promoters have concluded that in addition to neutralising surface acidity, alkali metal ions might promote $H_2$ spillover, inhibit coke deposition and increase the fraction of exposed metallic Pt surface after coke deposition [15,31–37].

The open literature is rather meagre on studies concerning $H_2$ production by fuel dehydrogenation, although the activity of Pt–Sn/$\gamma$-$Al_2O_3$ based catalysts in cyclohexane dehydrogenation and Pt/$\gamma$-$Al_2O_3$ based materials in Jet A-1 fuel dehydrogenation have been examined [14]. On the other hand, the activity of Pt–Sn/$\gamma$-$Al_2O_3$ based materials as catalysts for Jet A-1 fuel dehydrogenation seems not to have been investigated. The aim of the present work was the study of the partial dehydrogenation of Jet A-1 fuel on Pt–Sn based catalysts to produce $H_2$ to feed an on-board (aircraft) proton exchange membrane fuel cell.

## 2. Experimental

### 2.1. Catalyst preparation

Catalysts 5% wt.Pt-1% wt.Sn/$\gamma$-$Al_2O_3$ and 5% wt.Pt-1% wt.Sn-1% wt.Na/$\gamma$-$Al_2O_3$ (hereinafter denoted JM004 and JM007 respectively), were prepared by successive impregnations of Pt and Sn active phases. The $\gamma$-$Al_2O_3$ support (Degussa) was impregnated with a solution of hexachloroplatinic acid (Johnson Matthey), and the resulting product dried under reduced pressure in a rotary evaporator, then further dried at 110 °C for 2 h and finally calcined in air at 500 °C (10 °C/min) for 8 h. For part of the sample, a second impregnation was made with a solution of $SnCl_2 \cdot H_2O$ (Alfa Aesar), and the same drying and calcination procedure was performed. For the other part of the sample, the second impregnation was made with a solution of $SnCl_2 \cdot H_2O$ (Alfa Aesar) and $NaNO_3$ (BDH), before drying and calcining as above.

### 2.2. Catalyst characterization

X-ray powder diffraction (XRPD) patterns were recorded using a Philips PW 1050/81 goniometer, equipped with a PW 1710 unit, using Cu-K$\alpha$ radiation ($\lambda = 0.15418$ nm, 40 kW, 25 mA).

$N_2$ adsorption/desorption isotherms were obtained using a Micromeritics ASAP 2020 M P volumetric adsorption system operating at 77 K. The samples were pre-treated by outgassing at 150 °C for 12 h under secondary vacuum. Specific surface area and mean pore diameter were calculated from the adsorption and desorption branches of the isotherms, respectively. Measurements of surface acidity were performed by thermoprogrammed desorption of ammonia ($NH_3$-TPD) in an Autochem 2910 by Micromeritics equipped with a TCD detector. The samples were submitted to a flow of pure $NH_3$ at 100 °C for 1 h, and then flushed with He at 100 °C for 1 h. $NH_3$ was desorbed from the sample surface by heating to 900 °C under 30 ml/min He flow.

Transmission Electron Microscopy (TEM) investigations were performed using a JEOL 1200 EX microscope. The samples in powder form were reduced in $H_2$ at 350 °C for 4 h. They were then dispersed in ethanol and spread on a mica sheet. The dispersed powder was covered with a film of carbon and immersed in HF solution. The result was a carbon replica of the original structure containing only the metal (Pt and Sn) particles.

SEM/EDS analyses were performed using an EVO 50 Series Instrument (LEO ZEISS) equipped with an INCAEnergy 350 EDS

micro-analysis system and INCASmart-Map for imaging the spatial variation of elements in a sample (Oxford Instruments Analytical). The accelerating voltage was 25 kV, the beam current 1.5 nA, and the spectra collection time 100 s. Analyses were conducted on cut pellet lapped with 3 μm diamond spray. Samples were not pre-treated and analyses were performed at 90 Pa.

Thermal-programmed measurements were performed using a Thermoquest TPDRO1100 instrument. Calcined samples were loaded in a quartz reactor and pre-treated in nitrogen at 150 °C for 30 min to eliminate weakly adsorbed species. After cooling to room temperature, $N_2$ was replaced by the analysing gas [5%(v/v) $H_2$ in argon for reduction tests, 5%(v/v) $O_2$ in He for oxidation], and the temperature was increased up to 500 °C (10 °C/min). The samples were finally held at 500 °C for 20 min. Cyclic TPR/TPO/TPR tests were also carried out, whereby the samples were first reduced, then re-oxidized and then reduced a second time following the above protocol.

### 2.3. *Catalytic activity tests*

Preliminary catalytic activity tests were performed using 4.5 $cm^3$ of catalyst in a pressurised fixed bed flow reactor in line with a GC system (Agilent Technologies 6890N) equipped with TCD and FID detectors and two HP-PLOT Molesieve 5A and HP-PLOT/Q columns.

After purging, the system was pressurised with argon to 0.5 MPa and the reactor was heated from room temperature to the operating temperature; as soon as the operational temperature was reached, the fuel pump introduced the fresh fuel through the system at the desired flow rate (0.5 ml/min).

Temperature and pressure were continuously monitored up- and down-stream of the reactor. The exit stream of the reactor consisted of a two-phase mixture of $H_2$ rich gas (with some light hydrocarbons) and partially dehydrogenated liquid fuel, which was cooled to ca. 28 °C by a water cooler. The stream then entered a phase separator where liquid phase and gas phase were separated gravimetrically; the liquid phase was collected at the end of each experiment in a fuel collection tank. The gas phase stream was continuously sent out of the system through a back-pressure regulator (EL-PRESS® P-702C) from Bronkhorst, to the GC system, where a gas sample was taken every 10 min to perform $H_2$ and hydrocarbon analyses.

The reactor was shut off under Ar flow to maintain the pressure, purge the gases and collect the liquid streams. If the experiment were to be continued the following day, the system was kept under Ar overnight at 0.5 MPa. The catalytic activity tests were conducted at 350 °C at 0.5 MPa under two different types of feed: Jet A-1 fuel and desulfurised (3 ppm S) Jet A-1 fuel (Sulfur Free Kerosene: SFK). Tests with SFK Jet A-1 fuel were conducted over 2 days shutting-off and starting-up again the reactor without changing the catalytic bed for each catalyst.

## 3. Results and discussion

### 3.1. *Structural and surface characterisation*

The diffraction patterns of fresh and used JM004 and JM007 sample are shown in Fig. 1(a–c) and (d–f), respectively. Crystalline Pt and $SnO_2$ phases in addition to $\gamma$-$Al_2O_3$ and graphite (used as lubricant and cohesiveness agent in the pellets) are the main phases detected in the fresh samples. The spent samples show diffraction lines of Pt–Sn alloys indicated as $Pt_xSn_y$, while signal attributable to $SnO_2$ are detected.

The surface area of sample JM004 decreases from 184 $m^2/g$ for the fresh catalyst to 161 $m^2/g$ and 159 $m^2/g$ after reaction with Jet A-1 kerosene and desulfurised Jet A-1 kerosene respectively (Table 1). The JM007 catalyst has even more stable surface area values: 163 $m^2/g$ for the fresh sample, 161 $m^2/g$ for the sample tested with Jet A-1 kerosene and 157 $m^2/g$ after the test with desulfurised Jet A-1 kerosene.

The decrease of mean pore diameter is about 6% for JM004 after reaction either with Jet A-1 kerosene or SFK Jet A-1 kerosene. JM007 shows 6% of variation (like JM004) when tested with Jet A-1 kerosene, while it seems not to be affected by testing with desulfurised Jet A-1 kerosene.

Surface area and pore size values can be affected by rearrangement of the metal particle distribution, with the formation of clusters and poisoning by coke deposition. XRD analyses suggest that the addition of $Na^+$ ions to the catalyst formulation has a positive effect, inhibiting cluster formation.

The $NH_3$-TPD profiles of JM004 and JM007 are shown in Fig. 2, and the values of acidity (μmoles of $NH_3$/g of catalyst) derived from these plots are collected in Table 1.

Total acidity is lower for the support alone (204 μmoles of $NH_3$/g) then for JM004 and JM007. This effect is due to the fact that Pt is able to complex and decompose ammonia [38]. Analyzing results obtained in terms of total amount of ammonia desorbed and curve profile for samples containing Pt and support it is possible to explain acidic properties of samples as reported below.

Ammonia desorption from JM004 gives rise to three peaks in the range of temperature at 187, 296 and 480 °C, revealing the presence of both Lewis and Brönsted acid sites with different acidic strengths. In contrast, only two peaks at 189 and 290 °C are detected for JM007. Comparison of the $NH_3$-TPD curves for JM004 and JM007 indicates that the signal at 189 °C, ascribable to $NH_3$ desorption from weak acid sites, does not change in position or intensity by adding Na to the catalyst composition. A slight shift towards lower temperature for the second peak maximum is observed for JM007 while for JM004 the peak at 296 °C is the result of the contribution of medium strength Lewis and Brönsted acid sites. The addition of $NaNO_3$ mainly affects the Brönsted acidity, resulting in a decrease of the temperature and intensity of the signal. Finally, the absence of the peak at 480 °C in the $NH_3$ desorption curve of JM007 is evidence of the effect of the addition of sodium ions on strong acid sites. A further $NH_3$-TPD analysis performed on the support alone doped with 1% of $Na^+$ ions shows a decrease of total surface acidity of about 10% in line with the above data.

SEM-EDS analysis was used to provide information on the metal distribution in the fresh and the used catalysts. The catalyst pellets were cut in order to evaluate Pt and Sn concentrations and their radial distribution, i.e. from the edge to the centre. Attention is focused mainly on the fresh and used JM007 samples but similar results were obtained for JM004 samples. Fig. 3a shows SEM micrographs and EDS

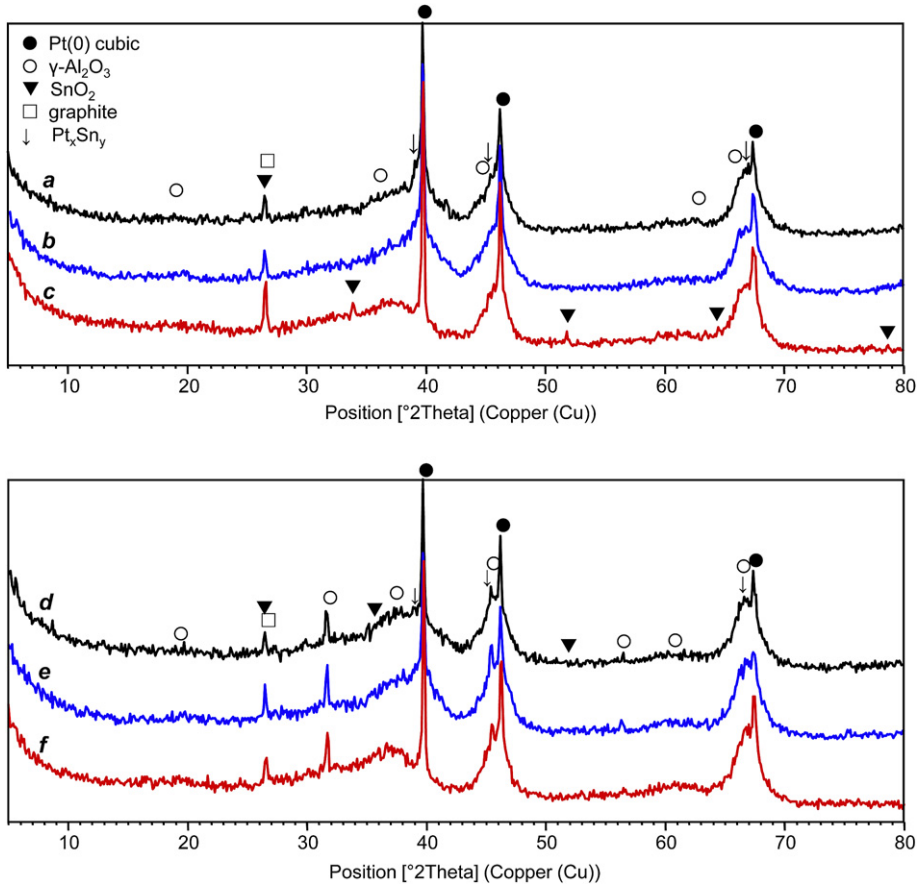


**Fig. 1 – XRD patterns of: a) spent JM004 SFK Jet A-1, b) spent JM004 Jet A-1, c) fresh JM004, d) spent JM007 SFK Jet A-1, e) spent JM007 Jet A-1, f) fresh JM007.**

analysis results of a fresh sample of JM007 carried out along the cut pellet (centre, near the edge and on the edge); the content of both Pt and Sn changes significantly moving from the centre to the external surface of the pellet. In detail, the Pt content is slightly lower than that expected in the centre of the pellet and higher at the edge, whereas the Sn is preferentially located at the edge. These results are confirmed by EDS metal maps of Sn and Pt shown in Fig. 3b, where a layer of Sn can be detected edge of the pellet. In addition, Pt aggregates of dimension ~10 μm can be detected mainly near to the surface of the pellet, while are not present, or are notably smaller, in the centre of the pellet, as shown in Fig. 3c.

**Table 1 – Number of acid sites and surface area and pore size of fresh and spent JM004 and JM007.**

| | | Surface acidity (μmol. $NH_3$/g) | BET Specific Surface Area ($m^2$/g) | Pore diameter (nm) | Pt Particle size (nm)[a] |
|---|---|---|---|---|---|
| JM004 | Fresh | 284 | 184 | 5.1 | 2 |
| | Spent Jet A-1 | – | 161 | 4.7 | 4 |
| | Spent SFK | – | 159 | 4.8 | 4–12 |
| JM007 | Fresh | 256 | 163 | 5.0 | 3 |
| | Spent Jet A-1 | – | 161 | 4.7 | 4 |
| | Spent SFK | – | 157 | 5.0 | 4 |

a Measured by TEM.

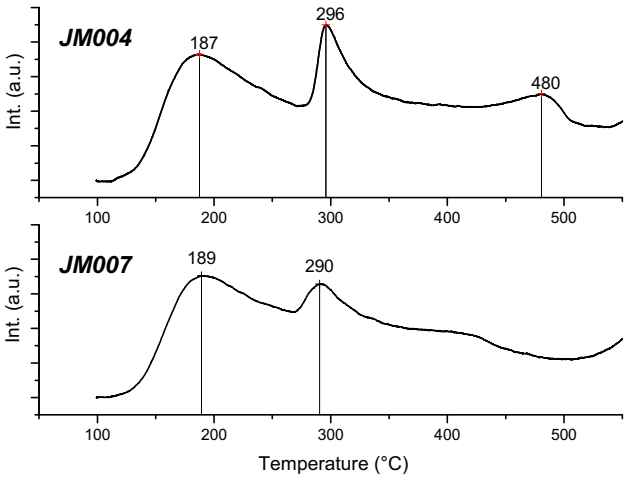


**Fig. 2 – $NH_3$-TPD profiles of JM004 and JM007.**

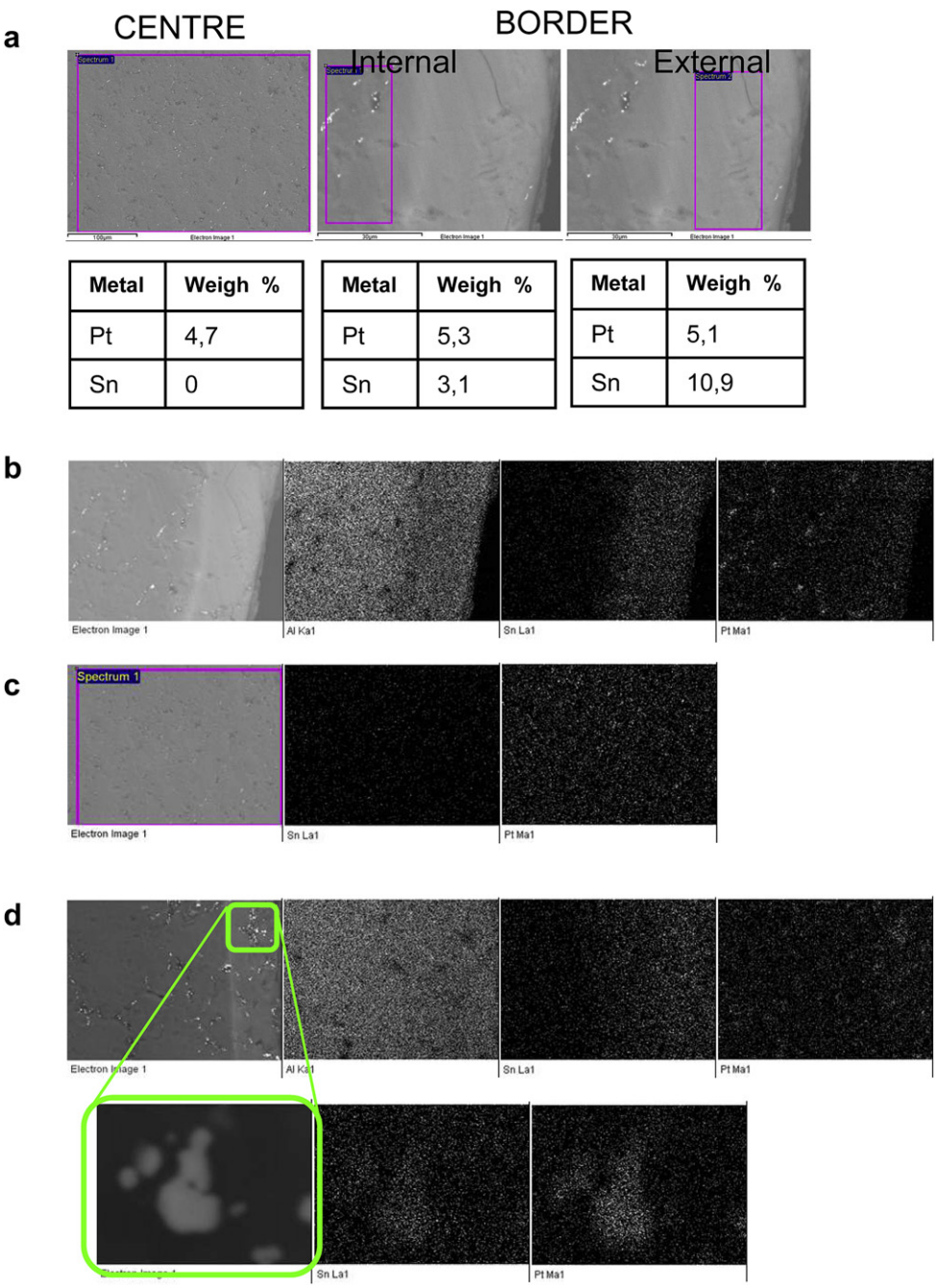


**Fig. 3 – a) SEM micrographs of fresh JM007 along the radius (from the edge to the centre) of the pellet and semi-quantitative average content of Pt and Sn calculated from EDX analysis; b) SEM micrograph of the edge of the pellet of fresh JM007 and EDX metal map; c) SEM micrograph of the centre of the pellet of fresh JM007 and EDX metal map; d) SEM micrograph of the edge of the pellet of JM007 after catalytic test with JetA-1 fuel and EDX metal map.**

Analysing the results reported in Fig. 3d of the spent JM007 after being tested for Jet A-1 dehydrogenation at 350 °C and 0.5 MPa, it is possible to observe the same Pt and Sn distribution as in the fresh sample, although the aggregates increase both in terms of number and dimension, mainly near to the pellet edge. EDS analysis on the aggregates observed after the catalytic test (see Fig. 3d) reveals the presence of both Pt and Sn, probably forming an alloy, as detected by XRD. This effect could be due to a migration of Sn towards the surface of Pt particles during the catalytic tests. As reported by Lieske et al. [39], formation of Pt–Sn alloy on $\gamma$-$Al_2O_3$ depends only on Sn concentration and not that of Pt(0), thus these Pt–Sn aggregates are present only near to the surface of the pellet where Sn is presents in large amount. Pt(0) catalyses the reduction of SnO to Sn(0), also stabilising it as an alloy.

The morphological properties of the metal particles in the fresh and spent catalysts were investigated by TEM. Representative TEM micrographs of the fresh JM004 and JM007

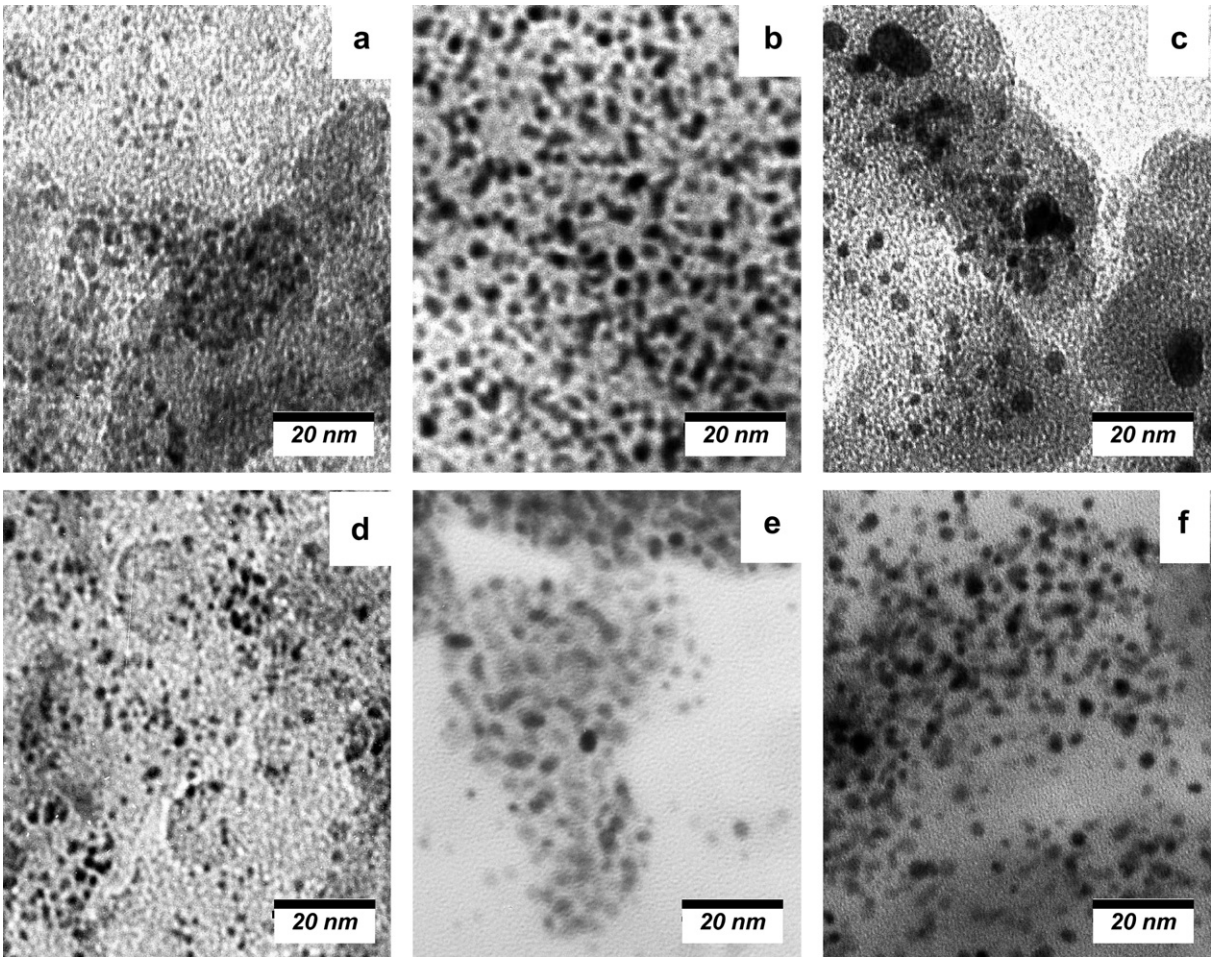


**Fig. 4 – TEM micrographs of: a) JM004 fresh, b) JM004 spent (tested under Jet A-1), c) JM004 spent (tested under SFK Jet A-1), d) JM007 fresh, e) JM007 spent (tested under Jet A-1), f) JM007 spent (tested under SFK Jet A-1).**

samples, as well as the corresponding spent samples after testing at 350 °C at 0.5 MPa feeding Jet A-1 or desulfurised kerosene Jet A-1 fuels, are shown in Fig. 4. For the fresh JM004 sample (Fig. 4a), the metal particles are homogeneously dispersed, with a diameter of ca. 2 nm. The TEM image of JM004 after the test with Jet A-1 fuel (Fig. 4b), shows that the particles, while still homogeneously dispersed, have ripened to a diameter of ca. 4 nm. After the tests with SFK Jet A-1, even more significant growth of the metal particles was observed, with formation of bigger clusters of size between 4 and 12 nm (Fig. 4c). In contrast, the calculated mean particle size of the JM007 fresh (Fig. 4d) and spent (Fig. 4e, f) catalysts is little

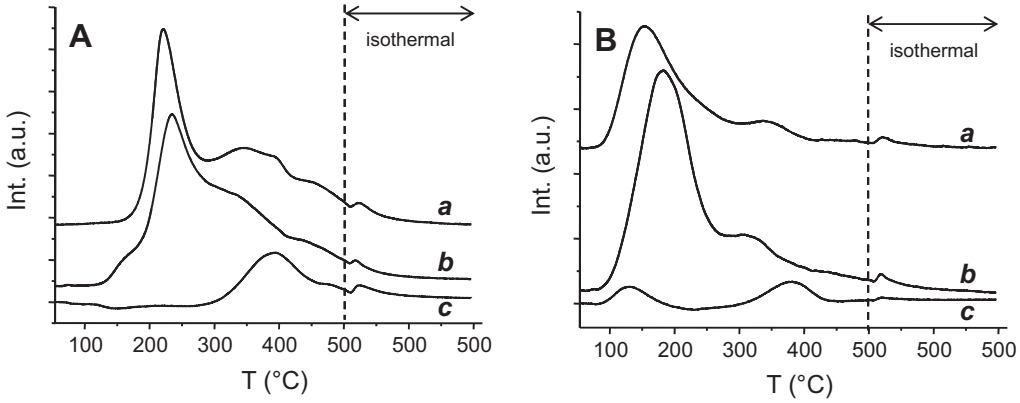


**Fig. 5 – TPR and TPO profiles A: $H_2$-TPR of a) fresh JM004, b) fresh JM007, c) 1%Pt/$\gamma$-$Al_2O_3$; B: $H_2$-TPR after previous $O_2$-TPO run of a) fresh JM004, b) fresh JM007, c) 1%Pt//$\gamma$-$Al_2O_3$.**

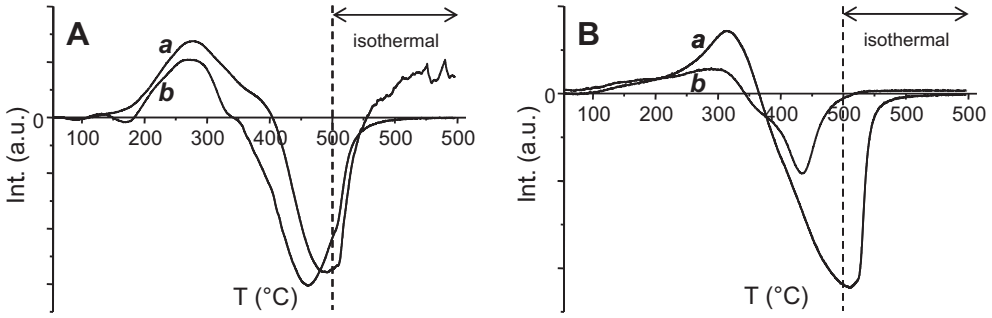


**Fig. 6 – A: $H_2$-TPR of spent JM007 tested under a) SFK Jet A-1, b) Jet A-1. B: $O_2$-TPO of spent JM007 tested under a) SFK Jet A-1, b) Jet A-1.**

changed, being 3 nm for the fresh catalyst and 4 nm for the two spent samples. The addition of sodium to the Pt–Sn formulation therefore stabilises the dispersion of metal particles [37].

The redox properties of the fresh and used catalysts were investigated by thermally programmed reduction with hydrogen (TPR) and oxidation using oxygen (TPO). The reduction profiles of JM004, JM007 and a reference sample (1% wt.Pt-$Al_2O_3$) are given in Fig. 5A (curves a, b and c respectively). In the reduction profile of the reference sample, only a broad peak can be observed, which extends over the range 290–500 °C and is centred at 390 °C. The shape of the peak suggests contributions of multiple components; the low temperature portion could be attributed to the reduction of Pt (IV) to Pt(0) [15,40,41], although the temperature is rather high compared to previously reported data [42,43]. A thin layer of partially reduced Pt possibly hinders $H_2$ diffusion towards the core of the particle during the reduction, while strong interaction between Pt(II) and the support may also increase the temperature of reduction of Pt(IV) to Pt(0) [41,44,45]. Furthermore, the reduction of oxochlorinated platinum species is known to result in $H_2$ consumption in the range 250–400 °C [41,46,47]. For JM004 and JM007, $H_2$ consumption occurs in the range 130–500 °C resulting in TPR profiles that are more complex than for the 1%Pt-$Al_2O_3$ reference. In the case of JM004, the hydrogen consumption culminates at 220 °C, while second maxima appear between 280 and 410 °C, where two features can be distinguished at 350 and 390 °C, with a shoulder at 450 °C. The TPR profile of JM007 shows a similar trend, but with an additional shoulder at 160 °C, the maximum intensity being observed at 230 °C, second maximum in the range 280–410 °C and a shoulder at 450 °C.

The complexity of the peak shape indicates that several different Pt and Sn surface species are present. The main peak at 220 °C for JM004 and 230 °C for JM007 is attributed mainly to reduction of Pt(IV), although Sn(IV) reduction also may contribute. In fact, the TPR profile of Sn(IV) usually shows two maxima, in the range 200–300 °C and 380–550 °C [15,39,46,47] in our case Sn(IV) reduction occurs at lower temperature due to the catalytic effect of Pt, which activates $H_2$ reduction of $SnO_2$, leading to the formation of alloy or bimetallic clusters [15,39,46,47].

Therefore the complex feature in the range 280–410 °C and the shoulder at 450 °C, for both samples, may be the result of the $H_2$ uptake to reduce separate Pt(II) or Sn(II) species strongly interacting with the support, or Pt oxochlorinated species [39,42,46,47].

The further $H_2$-TPR profiles after TPO treatment are shown in Fig. 5B. The TPR profile of the reference sample (1% wtPt-$Al_2O_3$, Fig. 5B-c) shows two peaks, including a new one at 130 °C, not observed in the first TPR. This feature at low temperature may be ascribed to the reduction of Pt(IV) weakly interacting with the support, whereas the peak at higher temperature, like for the TPR profile shown in Fig. 5A-c, may be related to a core and shell reduction, to the formation of Pt (II) species strongly interacting with the surface or to the reduction of oxochlorinated Pt species [39–41,44,45].

The TPR profiles after TPO treatment of JM004 and JM007 catalysts, reported in Fig. 5B-a and b, are broadly similar to those of Fig. 5A. In particular, an intense peak of $H_2$ consumption at 150 °C and 180 °C for JM004 and JM007 may be associated to the reduction of Pt(IV) species. The higher temperature than for reference 1% wt.Pt-$Al_2O_3$ may indicate a stronger interaction of Pt(IV) species with the alumina support, or with Sn(IV)/$Al_2O_3$ or Sn(II)/$Al_2O_3$ species [15]. $H_2$ consumption at 300 °C for JM007 and 340 °C for JM004 may be related to the reduction of Pt(II) or Sn(II) species stabilised on the support or to that of oxochlorinated Pt species. The re-oxidation step at 500 °C may favour the migration of Sn toward Pt, resulting in an intimate mixing between Pt and Sn and facilitating the reduction of $SnO_2$ [39]. These conclusions are in

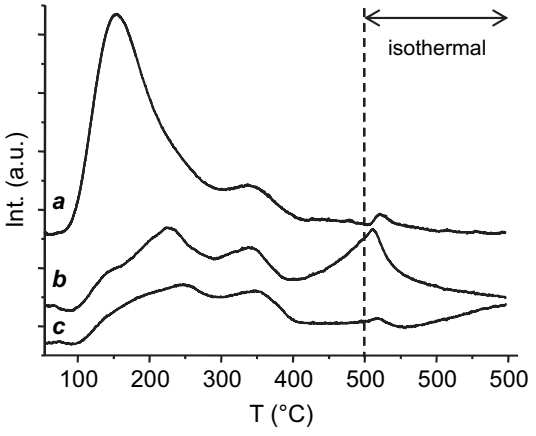


**Fig. 7 – $H_2$-TPR after previous $O_2$-TPO run of JM007 a) fresh, b) tested under Jet A-1, c) tested under SFK Jet A-1.**

**Table 2 – Catalytic activity results of JM004 and JM007 for partial dehydrogenation of Jet A-1 and SFK Jet A-1 at 350 °C, 5 bar.**

| | | $H_2$ production rate ($NL_{H_2}$ $kg^{-1}$ $hr^{-1}$) | Conv. to $H_2$ (%) | Conv. to $Hc_{gas}$ (%) | CH4 (% of $HC_{gas}$) | C2 (% of $HC_{gas}$) | C3 (% of $HC_{gas}$) | C4 (% of $HC_{gas}$) | C5 (% of $HC_{gas}$) | C6 (% of $HC_{gas}$) | $H_2$ purity (%) |
|---|---|---|---|---|---|---|---|---|---|---|---|
| *JM004* | | | | | | | | | | | |
| Jet A-1 | | 7 | 0.03 | n.a | n.a | n.a | n.a | n.a | n.a | n.a | n.a |
| SFK Jet A-1 | Day 1 | 45 | 0.4 | 0.2 | 87.7 | 2.6 | 2.0 | 2.2 | 1.8 | 3.7 | 95.7 |
| | Day 2 | 38 | 0.3 | 0.3 | 87.5 | 2.6 | 1.9 | 2.2 | 2.2 | 3.6 | 93.4 |
| *JM007* | | | | | | | | | | | |
| Jet A-1 | | 6.8 | 0.12 | n.a | n.a | n.a | n.a | n.a | n.a | n.a | n.a |
| SFK Jet A-1 | Day 1 | 132 | 1.3 | 1.4 | 97.1 | 0.6 | 0.4 | 0.5 | 0.5 | 0.9 | 92.1 |
| | Day 2 | 38 | 0.4 | 0.4 | 91.1 | 0.4 | 0.3 | 0.6 | 3.3 | 4.2 | 91.4 |

agreement with the shift to lower temperature (300–340 °C) of the peaks noted at 350–450 °C in Fig. 5A, and are compatible with the observations by SEM-EDS. It may be concluded from the TPR results that the surface of fresh JM004 and JM007 samples comprises Pt(IV) and Sn(IV) species weakly interacting with the alumina support, $Pt^0$ (confirmed by XRD), Pt–Sn alloy particles or bimetallic clusters, Pt(II) and Sn(II) species strongly stabilised at the support surface, and oxochlorinated Pt species, according to the literature [15,39,41,46,47].

The used catalysts were imbibed by the jet fuel from the catalytic tests, since no cleaning step was used before TPR analysis. A negative peak is observed at around 460 °C for JM007 both after the test with Jet A-1 fuel (Fig. 6A-b) and with SFK Jet A-1 fuel (Fig. 6A-a), due to $H_2$ production by dehydrogenation of adsorbed fuel on the catalyst. In the oxidation step (Fig. 6B), a negative peak is observed due to CO and $CO_2$ production by combustion of both adsorbed jet-fuel and coke. Fig. 7 shows the $H_2$-TPR profiles after oxidation of the spent JM007 samples tested with Jet A-1 (Fig. 7b) and SFK Jet A-1 fuel (Fig. 7c) compared to the fresh JM007 sample (Fig. 7a). In all cases, the intensity of the peak at 150 °C related to Pt reduction strongly decreases, probably due either to a not sufficient concentration of $O_2$ to burn adsorbed jet fuel and re-oxidize all the Pt, or to an increase of Pt particle size as observed by SEM, such that the surface metal area decreases and the core of the particle becomes more difficult to reduce. Finally, the peak of reduction of Sn is absent, probably due to the sintering of the particles or formation of Pt/Sn alloy or cluster, as observed by SEM-EDS and XRD.

### 3.2. *Catalytic activity tests*

The results of the preliminary catalytic activity tests conducted with JM004 and JM007 at 0.5 MPa at 350 °C on Jet A-1 and SFK Jet A-1 kerosene for 48 h (shutting down and starting up the reactor overnight) are summarised in Table 2; an average molecular formula $C_{12}H_{26}$ for Jet A-1 was used in calculations [48–50]. On this basis the kerosene conversion to $H_2$ was calculated using Eq. (1):

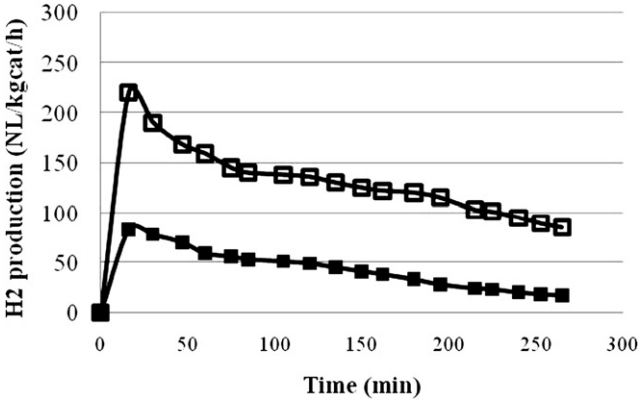


**Fig. 8 – $H_2$ production rate versus time of stream. JM004 (full symbol), JM007 (open symbol). Reaction condition: 350 °C, 5 bar SFK.**

**Table 3 – Fuel properties of fresh and partially dehydrogenated SFK Jet A-1 kerosene.**

| Property | Units | ASTM Method | Fresh Kerosene Jet A-1 TOTAL (France) | Dehydro-Kerosene Jet A-1 Bayern Oil (Germany) | ASTM D1655-07 |
|---|---|---|---|---|---|
| Acidity | mg KOH/g | D3242 | 0.001 | 0.002 | 0.10 (max) |
| Aromatics | Vol % | D1319 | 15.6 | 20.1 | 25 (max) |
| Final Boiling Point | °C | D86 | 252.5 | 248.7 | 340 (max) |
| Flash point | °C | D56/D3828 | 41.5 | 51.5 | 38 (min) |
| Density (@15 °C) | $Kg/m^3$ | D1298/D4052 | 788.1 | 805.7 | 775 to 840 (max) |
| Freezing point | °C | D5972/D7153/ D7154/D2386 | −58.6 | −59 | −47 (max) |
| Viscosity (@ −20 °C) | $mm^2/s$ | D445 | 2.873 | 3.821 | 8.0 (max) |
| Net Heat of Combustion | MJ/kg | D4529/D3338/ D4809 | 43.356 | 43.15 | 42.8 (min) |
| Naphtalenes | Vol % | D1840 | 0.3 | 0.5 | 3.0 (max) |
| Filter Pressure Drop | mmHg | D3241 | 0 | 0 | 25 (max) |
| Visual method | | D3241 | No peacock or abnormal color deposits | No peacock or abnormal color deposits | No peacock or abnormal color deposits |

$$\text{Conversion to } H_2\ (\%) = \frac{n\,H_2 out}{n\,H_2 in} \times 100 \quad (1)$$

The type of kerosene fed to the catalyst strongly affects the amount of $H_2$ produced during the first 8 h. With Jet A-1 kerosene the $H_2$ production rate does not exceed 7 NL $kg_{cat}^{-1}$ $h^{-1}$, which corresponds to 0.1–0.3% of conversion of the reactant mixture to $H_2$. The $H_2$ production rate with SFK Jet A-1 kerosene is 45 NL $kg_{cat}^{-1}$ $h^{-1}$ over JM004 catalyst and 132 NL $kg_{cat}^{-1}$ $h^{-1}$ over the JM007 catalyst, corresponding to 0.4% and 1.3% of conversion of SFK Jet A-1 kerosene to $H_2$ for JM004 and JM007 respectively. Fig. 8 shows the trends of the production rate versus time on stream for JM004 and JM007; the S-content in Jet A-1 kerosene affects the $H_2$ production rate. In particular, it is reasonable to conclude that fast deactivation of the surface active sites of both JM004 and JM007 catalysts is due to the poisoning by the S present in the Jet A-1 kerosene stream. The presence of sodium in JM007 has a positive effect on the catalyst performance in terms of $H_2$ production during the first day of test, both due to its influence on the catalyst acidity or by avoiding metal particle sintering. Despite this, the activity is lower on the second day, with $H_2$ production of 38 NL $kg_{cat}^{-1}$ $h^{-1}$ for both JM007 and JM004.

The formation of light hydrocarbons (from C1 to C6) is evidence of the occurrence of undesired side reactions, like cracking. C1–C6 compounds remain rather low when feeding SFK Jet A-1 kerosene: about 1.4% with JM007 and 0.2% with JM004 during the first day, falling to 0.3% and 0.4% respectively on the second day. According to Table 2, $CH_4$ is the most abundant light hydrocarbon in the outlet stream, 87–88% of the total volume using JM004 (97% with JM007 on day one) and 91% on the second day of test. The production of $C_2$–$C_4$ hydrocarbons is four times higher using JM004 than JM007 catalyst, without any particular change with time on stream. These results indicate that $H_2$ production follows a similar trend to the conversion to gaseous hydrocarbons (while the production of $C_5$, $C_6$ hydrocarbons tends to decrease), indicating that also cracking reactions contribute to $H_2$ production. The extent of cracking reactions on JM004 seems to be lower than on JM007 during the first day of test. The occurrence of cracking reactions results in a decrease of $H_2$ purity which is 92% when the $H_2$ production rate reaches its maximum of 132 NL $kg_{cat}^{-1}$ $h^{-1}$.

These preliminary results do not allow any discrimination between cracking and dehydrogenation reactions. Multiple factors may contribute to the loss of activity of JM007, including catalyst deactivation by coke deposition or decrease in metal dispersion on the surface. The formation of larger metal clusters results in a drop in active area giving a lower catalytic activity as a consequence. One target of this work was to recover a dehydrogenated fuel still having the same fuel properties of the reactant blend fuel; thus a characterisation of the blend condensed at the outlet (Table 3) is reported, showing that its composition still lies within the limits of the ASTM D1655-07 specifications.

## 4. Conclusions

The Pt–Sn catalysts 5% wt.Pt-1% wt.Sn/$\gamma$-$Al_2O_3$ and 5% wt.Pt-1% wt.Sn-1%Na/$\gamma$-$Al_2O_3$ prepared by successive impregnations of the metal salts on $\gamma$-alumina pellets have a gradient of active metals from the edge to centre due to different diffusion properties. $Pt^0$ is present in highest concentration in the external part of the pellet, while $SnO_2$ is present only at external part of the pellet. These materials are active catalysts for the partial dehydrogenation of Jet A-1 (300 ppm S) and desulfurised (3 ppm S) Jet A-1 fuel, although the catalysts are not thio-tolerant and $H_2$ production decreases rapidly with time on stream. A catalyst co-impregnated with sodium nitrate gave the highest and most sustained $H_2$ generation, the presence of sodium inhibiting the metal particle aggregation and/or decreasing the acidity of the catalyst surface. Furthermore, the condensed liquid at the exit stream retains the useful characteristics of Jet A-1. Coking and sulfur

poisoning appear the main drawbacks to overcome for a future improvement of catalyst activity and stability in the on-board $H_2$ production by partial dehydrogenation of jet-fuels.

## Acknowledgement

This work was performed as part of the GreenAir project, EC contract number 233862. The authors thank Erich Erdle for enlightening discussions and his contributions to this work.

## REFERENCES

[1] Satyapal S, Petrovic J, Read C, Thomas G, Ordaz G. The U.S. department of energy's national hydrogen storage project: progress towards meeting hydrogen-powered vehicle requirements. Catal Today 2007;120:246–56.
[2] Ross DK. Hydrogen storage: the major technological barrier to the development of hydrogen fuel cell cars. Vacuum 2006; 80:084–1089.
[3] Aardahl CL, Rassat SD. Overview of systems considerations for on-board chemical hydrogen storage. Int J Hydrogen Energy 2009;34:6676–83.
[4] Hellman HL, Van den Hoed R. Characterising fuel cell technology: challenges of the commercialisation process. Int J Hydrogen Energy 2007;32:305–15.
[5] Chalk SG, Miller JF. Key challenges and recent progress in batteries, fuel cells, and hydrogen storage for clean energy systems. J Power Sources 2006;159:73–80.
[6] Biniwale RB, Rayalu S, Devotta S, Ichikawa M. Chemical hydrides: a solution to high capacity hydrogen storage and supply. Int J Hydrogen Energy 2008;33:360–5.
[7] Elena D. An overview of advanced materials for hydrogen storage. J Mat Process Technol 2005;162-163:169–77.
[8] Sakintuna B, Lamari-Darkrim F, Hirscher M. Metal hydride materials for solid hydrogen storage: a review. Int J Hydrogen Energy 2007;32:1121–40.
[9] Lazaro MP, Garcia-Bordejé E, Sebastian D, Lazaro MJ, Moliner R. In situ hydrogen generation from cycloalkanes using a Pt/CNF catalyst. Catal Today 2008;138:203–9.
[10] Okada Y, Sasaki E, Watanabe E, Hyodo S, Nishijima H. Development of dehydrogenation catalyst for hydrogen generation in organic chemical hydride method. Int J Hydrogen Energy 2006;31:1348–56.
[11] Saito Y, Aramaki K, Hodoshima S, Saito M, Shono A, Kuwano J, et al. Efficient hydrogen generation from organic chemical hydrides by using catalytic reactor on the basis of superheated liquid-film concept. Chem Eng Sci 2008;63:4935–41.
[12] Hodoshima S, Takaiwa S, Shono A, Satoh K, Saito Y. Hydrogen storage by decalin/naphthalene pair and hydrogen supply to fuel cells by use of superheated liquid-film-type catalysis. Appl Catal A Gen 2005;283:235–42.
[13] Rahimpour MR. Enhancement of hydrogen production in a novel fluidized-bed membrane reactor for naphtha reforming. Int J Hydrogen Energy 2009;34:2235–51.
[14] Wang B, Froment GF, Wayne Goodman D. CO-free hydrogen production via dehydrogenation of a Jet A hydrocarbon mixture. J Catal 2008;253:239–43.
[15] He S, Sun C, Bai Z, Dai X, Wang B. Dehydrogenation of long chain paraffins over supported Pt–Sn–K/$Al_2O_3$ catalysts: a study of the alumina support effect. Appl Catal A Gen 2009; 356:88–98.
[16] Hodoshima S, Hiroshi A, Yasukazu S. Liquid-film-type catalytic decalin dehydrogeno-aromatization for long-term storage and long-distance transportation of hydrogen. Int J Hydrogen Energy 2003;28:197–204.
[17] Kariya N, Fukuoka A, Ichikawa M. Efficient evolution of hydrogen from liquid cycloalkanes over Pt-containing catalysts supported on active carbons under "wet–dry multiphase conditions". Appl Catal A Gen 2002;233:91–102.
[18] Hodoshima S, Nagata H, Yasukazu S. Efficient hydrogen supply from tetralin with superheated liquid-film-type catalysis for operating fuel cells. Appl Catal A Gen 2005;292:90–6.
[19] Biniwale RB, Kariya N, Ichikawa M. Dehydrogenation of cyclohexane over Ni based catalysts supported on activated carbon using spray-pulsed reactor and enhancement in activity by addition of a small amount of Pt. Catal Lett 2005; 105:83–7.
[20] Kariya N, Fukuoka A, Utagawa T, Sakuramoto M, Goto Y, Ichikawa M. Efficient hydrogen production using cyclohexane and decalin by pulse-spray mode reactor with Pt catalysts. Appl Catal A Gen 2003;247:247–59.
[21] Yolcular S, Olgun O. Ni/$Al_2O_3$ catalysts and their activity in dehydrogenation of methylcyclohexane for hydrogen production. Catal Today 2008;138:198–202.
[22] Sebastian D, Bordejé EG, Calvillo L, Lazaro MJ, Moliner R. Hydrogen storage by decalin dehydrogenation/ naphthalene hydrogenation pair over platinum catalysts supported on activated carbon. Int J Hydrogen Energy 2008;33:1329–34.
[23] Wang Y, Shah N, Huggins FE, Huffman GP. Hydrogen production by catalytic dehydrogenation of tetralin and decalin over stacked cone carbon nanotube-supported Pt catalysts. Energy Fuels 2006;20:2612–5.
[24] Akamatsu K, Ohta Y, Sugawara T, Hattori T, Nakao S. Production of hydrogen by dehydrogenation of cyclohexane in high-pressure (1–8 atm) membrane reactors using amorphous silica membranes with controlled pore sizes. Ind Eng Chem Res 2008;47:9842–7.
[25] Dung Tien P, Satoh T, Miura M, Nomura M. Continuous hydrogen evolution from cyclohexanes over platinum catalysts supported on activated carbon fibers. Fuel Process Technol 2008;89:415–8.
[26] Li P, Huang Y, Chen D, Zhu J, Zhao T, Zhou X. CNFs-supported Pt catalyst for hydrogen evolution from decalin. Catal Comm 2009;10:815–8.
[27] Park YK, Ribeiro FH, Somorjai GA. The effect of potassium and tin on the hydrogenation of ethylene and dehydrogenation of cyclohexane over Pt(111). J Catal 1998;178:66–75.
[28] González-Marcos MP, Iñarra B, Guil JM, Gutiérrez-Ortiz MA. Development of an industrial characterisation method for naphtha reforming bimetallic Pt-Sn/$Al_2O_3$ catalysts through *n*-heptane reforming test reactions. Catal Today 2005; 107–108:685–92.
[29] González-Marcos MP, Iñarra B, Guil JM, Gutiérrez-Ortiz MA. Use of test reactions for the characterisation of bimetallic Pt–Sn/$Al_2O_3$ catalysts. Appl Catal A 2004;273:259–68.
[30] Passos FB, Aranda DAG, Schmal M. Characterization and catalytic activity of bimetallic Pt–In/$Al_2O_3$and Pt–Sn/ $Al_2O_3$Catalysts. J Catal 1998;178:478–88.
[31] Praserthdam P, Choungchaisukasam P, Assabumrungrat S, Mongkhonsi T. Role of Sn and K on hydrogen spillover on Pt/ $\gamma$-$Al_2O_3$ catalyst. J Chin Inst Chem Eng 2001;32:143–9.
[32] Wang L, Lin L, Zang T, Cai H. Enhancement of Pt–Sn/$Al_2O_3$ catalyst stability for butane dehydrogenation by modification with Sn and Li. React Kinet Catal Lett 1994;52: 107–11.
[33] Cortright RD, Dumesic JA. Effects of potassium on silica-supported Pt and Pt/Sn catalysts for isobutane dehydrogenation. J Catal 1995;157:576–83.
[34] Gokak DT, Basrur AG, Rajeswar D, Rao GS, Krishnamurthy KR. Lithium promoted Pt–Sn/$Al_2O_3$ catalysts

for dehydrogenation of *n*-decane: influence of lithium metal precursors. React Kinet Catal Lett 1996;59:315–23.
[35] Casella ML, Siri GJ, Santori GF, Ferretti OA, Ramirez-Corredores MM. Surface characterization of li-modified platinum/tin catalysts for isobutane dehydrogenation. Langmuir 2000;16:5639–43.
[36] Qiu AD, Fan YN, Ma YF, Wu PC, Chen Y. Effects of alkali promoters on catalytic properties of alumina-supported Pt–Sn catalysts for long-chain paraffin dehydrogenation. Chin J Catal 2001;22:343–7.
[37] Zhang Y, Zhou Y, Qiu A, Wang Y, Xu Y, Wu P. Effect of Na addition on catalytic performance of PtSn/ZSM-5 catalyst for propane dehydrogenation. Acta Phys Chim Sin 2006;22:672–8.
[38] Albertazzi S, Baraldini I, Busca G, Finocchio E, Lenarda M, Storaro L, et al. Noble metal containing Al/Ce/Mg pillared montmorillonite clay as catalysts in the hydrotreating of LCO fractions. Appl Clay Sci 2005;29:224–34.
[39] Lieske H, Völter J. State of tin in Pt–Sn/$Al_2O_3$ reforming catalysts investigated by TPR and chemisorption. J Catal 1984;90:96–105.
[40] Badano JM, Quiroga M, Betti C, Vera C, Canavese S, Colma-Pascual F. Resistance to sulfur and oxygenated compounds of supported Pd, Pt, Rh, Ru catalysts. Catal Lett 2010;137:35–44.
[41] Reyes P, Pecci G, Morales M, Fierro JLG. The nature of the support and the metal precursor on the resistance to sulphur poisoning of Pt supported catalysts. Appl Catal A Gen 1997; 163:145–52.
[42] Bocanegra SA, de Miguel SR, Borbath I, Margitflavi JL, Scleza OA. Behavior of bimetallic PtSn/$Al_2O_3$ catalysts prepared by controlled surface reactions in the selective dehydrogenation of butane. J Mol Catal A Chem 2009;301: 52–60.
[43] Alvarez-Galvan MC, Navarro RM, Rosa F, Briceno Y, Ridao MA, Fierro JLG. Hydrogen production for fuel cell by oxidative reforming of diesel surrogate: influence of ceria and/or lanthana over the activity of Pt/$Al_2O_3$ catalysts. Fuel 2008;87:2502–11.
[44] Lieske H, Lietz G, Spindler H, Voelter J. Reactions of platinum in oxygen- and hydrogen-treated Pt/$\gamma$-$Al_2O_3$ catalysts: I. temperature-programmed reduction, adsorption, and redispersion of platinum. J Catal 1983;81:8–16.
[45] Huizinga T, van Grondelle J, Prins R. A temperature programmed reduction study of Pt on $Al_2O_3$ and $TiO_2$. Appl Catal 1984;10:199–213.
[46] Carvalho LS, Pieck CL, Rangel MC, Fígoli NS, Grau JM, Reyes P, et al. Trimetallic naphtha reforming catalysts. I. properties of the metal function and influence of the order of addition of the metal precursors on Pt–Re–Sn/$\gamma$-$Al_2O_3$–Cl. Appl Catal A Gen 2004;269:91–103.
[47] Ballarini AD, Zgolicz P, Vilella IMJ, de Miguel SR, Castro AA, Scleza OA. n-Butane dehydrogenation on Pt, PtSn and PtGe supported on $\gamma$-$Al_2O_3$ deposited on spheres of $\alpha$-$Al_2O_3$ by washcoating. Appl Catal A Gen 2010;381: 83–91.
[48] Rachner M. The properties of kerosene Jet A-1. Koeln: DLR Mitteilung; 1998. pp. 98–101.
[49] MiRO, Mineraloelraffinerie oberrhein GMBH & Co. KG, June 2007, www.miro-ka.de/.
[50] Brown LF. A comparative study of fuels for on-board hydrogen production for fuel-cell-powered automobiles. Int J Hydrogen Energy 2001;26:381–97. 24.